





RESEARCH ARTICLE | MARCH 24 2025

Electrical activities of sulfur dopants in GaAs introduced by self-assembled molecular monolayers

Zhengfang Fan ; Yumeng Liu ; Yizhuo Wang ; Hao Wei ; He Li ; Shuwen Guo ; Li He ; Xiaochun Lai ; Yaping Dan  

 Check for updates

J. Appl. Phys. 137, 125102 (2025)

<https://doi.org/10.1063/5.0243124>


View Online


Export Citation

Articles You May Be Interested In

Transforming underground to surface mining operation – A geotechnical perspective from case study

AIP Conference Proceedings (November 2021)

Monthly prediction of rainfall in nickel mine area with artificial neural network

AIP Conference Proceedings (November 2021)

Estimation of Karts groundwater based on geophysical methods in the Monggol Village, Saptosari District, Gunungkidul Regency

AIP Conference Proceedings (November 2021)

24 March 2025 11:22:25



Nanotechnology & Materials Science



Optics & Photonics



Impedance Analysis



Scanning Probe Microscopy



Sensors



Failure Analysis & Semiconductors



Unlock the Full Spectrum.
From DC to 8.5 GHz.

Your Application. Measured.

Find out more

 Zurich Instruments

Electrical activities of sulfur dopants in GaAs introduced by self-assembled molecular monolayers

Cite as: J. Appl. Phys. 137, 125102 (2025); doi: 10.1063/5.0243124

Submitted: 9 October 2024 · Accepted: 19 February 2025 ·

Published Online: 24 March 2025



Zhengfang Fan,^{1,2} Yumeng Liu,^{1,2} Yizhuo Wang,¹ Hao Wei,² He Li,^{3,4} Shuwen Guo,^{1,5.a)} Li He,^{6,b)}
Xiaochun Lai,^{4,7} and Yaping Dan^{1,c)}

AFFILIATIONS

¹University of Michigan—Shanghai Jiao Tong University Joint Institute, Shanghai Jiao Tong University, Shanghai 200240, China

²Department of Micro/Nano Electronics, School of Electronic Information and Electrical Engineering, Shanghai Jiao Tong University, Shanghai 200240, China

³Shanghai United Imaging Healthcare Advanced Technology Research Institute Co., Ltd, Shanghai 201807, China

⁴Photonic Sensing and Imaging Lab, School of Biomedical Engineering, ShanghaiTech University, Shanghai 201210, China

⁵School of Energy and Materials, Shanghai Polytechnic University, Shanghai 201209, China

⁶State Key Laboratory of Superlattices and Microstructures, Institute of Semiconductors, Chinese Academy of Science, Beijing 100083, China

⁷Shanghai Clinical Research and Trial Center, Shanghai 201210, China

^{a)} Email: shuwen.guo@sjtu.edu.cn

^{b)} Email: heli2018@semi.ac.cn

^{c)} Author to whom correspondence should be addressed: yaping.dan@sjtu.edu.cn

ABSTRACT

Self-assembled molecular monolayer doping remains as a research focus for its nature of being conformal, nondestructive, and self-limiting. However, the carrying molecules may contaminate the substrate and electrically deactivate the dopants. In this work, we investigate the electrical activities of sulfur dopants in GaAs introduced by the self-assembled molecular monolayer doping technique. The results from secondary ion mass spectrometry and low-temperature Hall measurements show that the activation energy of sulfur dopants is 68 meV, and that 91% of these dopants introduced into GaAs by the self-assembled molecular monolayer doping technique are electrically active. The impact of the carrying molecular contamination is minimal. We employ this monolayer doping technique to create a PN junction diode on a p-type GaAs substrate. The PN junction diode exhibits an outstanding performance with an ideality factor of 1.26 and a rectification ratio up to 10^4 within the bias of ± 0.6 V.

© 2025 Author(s). All article content, except where otherwise noted, is licensed under a Creative Commons Attribution (CC BY) license (<https://creativecommons.org/licenses/by/4.0/>). <https://doi.org/10.1063/5.0243124>

INTRODUCTION

Self-assembled monolayer (SAM) doping has a wide range of applications in nanoscale semiconductor devices¹ and Fin Field-Effect Transistors (FinFETs).^{2,3} This technique enables precise control over dopant profiles, which is crucial for achieving optimal device performance. It has been successfully demonstrated for a wide range of n- and p-type dopants on silicon surfaces.^{3,4} Considerable

research has been conducted on the electrical activities of dopants in silicon,^{5,6} demonstrating its versatility and effectiveness. Recently, the method has been extensively applied to III-V semiconductors with exceptional transport characteristics, which make them particularly suitable for applications in transistors,^{7,8} high-speed nanoelectronics,^{9,10} and solar energy harvesting.¹¹

For III-V substrates, the self-assembled sulfur (S) monolayer is often used to passivate the surface to attain long-term stability.

For instance, Hedieh *et al.*¹² passivated GaAs surfaces to prevent re-oxidation by treating with the ammonium sulfide $(\text{NH}_4)_2\text{S}_x$ solution and found a ten-day stability in air via x-ray photoelectron spectroscopy (XPS). This long-term stability was attributed to the full coverage of sulfur monolayer on the GaAs surfaces because the sulfur monolayer has completely saturated the dangling bonds on GaAs surfaces, prohibiting the absorption of foreign atoms. What is more, the sulfur monolayer passivation has been demonstrated to improve the long-term stability of re-oxidized InGaAs,¹³ n-GaAs nanowires,¹⁴ AlGaAs/InGaAs transistors,¹⁵ and others.^{16,17} The sulfur monolayer passivation indicates sulfur atoms are directly bonded on the surface and, therefore, can be utilized as a controlled doping source. Ho *et al.*¹⁸ fabricated the n^+/p^+ tunneling diodes with electrically active sulfur concentrations of $8 \times 10^{18} \text{ cm}^{-3}$ via sulfur monolayer doping scheme in InAs, in order to demonstrate the nanoscale doping ability of the sulfur doping method. Kort *et al.*¹⁹ reported a non-destructive Raman spectroscopy study of electron–phonon coupling in sulfur monolayer doped $\text{In}_{0.53}\text{Ga}_{0.47}\text{As}$ and found the electrically active S concentration of $9.5 \times 10^{18} \text{ cm}^{-3}$ at a depth of 10 nm from the surface. To increase the active sulfur concentration, Yum *et al.*²⁰ studied the effect of the capping layer in sulfur monolayer doping on InGaAs and found the device with a SiN_x/BeO bi-layer cap exhibits a higher electrically active S concentration of $4.9 \times 10^{19} \text{ cm}^{-3}$ compared to the single capping layer. Mattson and Chhabal²¹ provided the understanding of the reactions involving dopant-containing monolayers, intermediate structures, and the role of capping layers in sulfur-passivated GaAs and found that an intermediate (2×1) surface reconstruction for S-passivated GaAs was observed before subsurface diffusion. They also investigated that the active sulfur dopants concentration exceeded 10^{20} cm^{-3} in GaAs, but not consider the contamination carrying by sulfur monolayer. It is well known that the carrying molecules in this technique introduce contamination to the underlying substrate and often electrically deactivate the dopants as we previously found in silicon.^{4,6,22,23} Whether the carrying molecules will electrically deactivate the sulfur dopants in GaAs remains unclear.

In this work, we demonstrated a self-assembled sulfur monolayer doping technique by grafting sulfur onto GaAs in the $(\text{NH}_4)_2\text{S}_x$ solution. The sulfur dopants were then driven into GaAs to create electrical doping effect by the rapid thermal annealing (RTA) process. The chemical absorption of the sulfur monolayer on GaAs surfaces was examined by XPS. The total number of dopants diffused into GaAs was analyzed by secondary ion mass spectroscopy (SIMS) and the source-limited diffusion model. Hall effect measurements were employed to find the electron concentration at different temperatures. The temperature dependent electron concentration was fitted with the dopant activation theory, from which we extracted the activation energy as 68 meV and the concentration of electrically active sulfur dopants as high as $4.4 \times 10^{14} \text{ cm}^{-2}$. We find that more than 91% of sulfur dopants in GaAs are electrically active, indicating that the impact of carrying molecules is minimal. In the end, a PN junction diode was fabricated by using the molecular monolayer doping technique on a p-type GaAs substrate. The PN junction diode exhibits an ideality of 1.26 and a rectification ratio of 10^4 within the bias of $\pm 0.6 \text{ V}$.

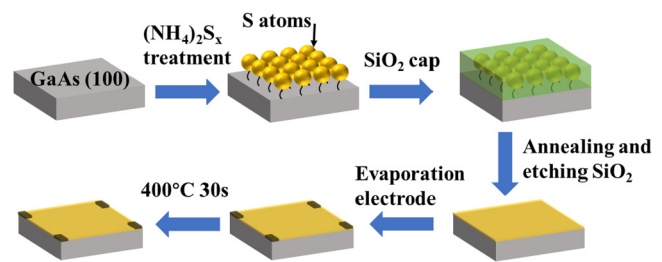


FIG. 1. Schematic of the SAM sulfur monolayer doping process using sulfur precursors on the GaAs substrate.

EXPERIMENTAL

The SAM sulfur monolayer doping process using sulfur precursors on the GaAs substrate is shown in Fig. 1. Intrinsic GaAs (100) wafers were chemically cleaned with acetone, isopropanol, and de-ionized water. For sulfur monolayer grafting, a saturated ammonium sulfide solution was prepared by adding 0.27 g excess sulfur to a 20 ml $(\text{NH}_4)_2\text{S}$ solution, which was stirred for 2 h to obtain a proper dissolution of sulfur excess. Prior to sulfur monolayer grafting, the native oxide was removed by immersion in a 3:1 solution of de-ionized water/HCl (37%) for 5 min followed by a 3 min de-ionized water rinse. Subsequently, the GaAs wafers were dipped into a saturated $(\text{NH}_4)_2\text{S}$ solution for 4 h at room temperature.²¹ After S monolayer formation on the GaAs surface, a 200 nm thick SiO_2 capping layer was sputtered onto the samples, followed by annealing at different temperatures to drive S atoms into GaAs. Finally, a layer of 5 nm germanium and 100 nm gold electrode were deposited on the surface of the samples by a vacuum thermal evaporator. After the evaporation, the samples were annealed at 400 °C for 30 s by RTA under an atmospheric pressure of N_2 to obtain Ohmic contact.¹⁶

RESULTS AND DISCUSSION

X-ray photoelectron spectroscopy was performed for the surface-functionalized sample as shown in Fig. 2, which shows the XPS spectra of Ga 2p, As 3d, and S 2p core levels of sulfur-passivated GaAs surfaces. In Fig. 2(a), a shoulder can be clearly observed on the higher binding energy side of the Ga 2p peak. After curve-fitting, a second peak with a chemical shift of 0.53 eV is observed, which is consistent with the formation of Ga–S bonds.²⁴ As shown in Fig. 2(b), the peak at 41.2 eV is related to Ga–As bonds, and As elemental is located at a binding energy of 42 eV, which is in good agreement with the literature.¹² Due to the overlap of Ga 3s and As 2p plasmon loss, the S 2p XPS spectra are more complex. Figure 2(c) clearly indicates several different chemical states, including the Ga 3s level (binding energy at 160 eV), the S 2p level (at 162 eV) and a plasmon satellite from the intense As 2p (at 158 eV).^{24,25} Collectively, these XPS data indicate that sulfur atoms occupy the dangling bonds at the surface of GaAs, indicating that sulfur atoms have been grafted on the GaAs surfaces.

After successfully grafting sulfur atoms onto the surfaces of GaAs, a 200 nm thick SiO_2 capping layer was sputtered onto the samples to act as a protective barrier layer during rapid thermal

24 March 2025 11:22:25

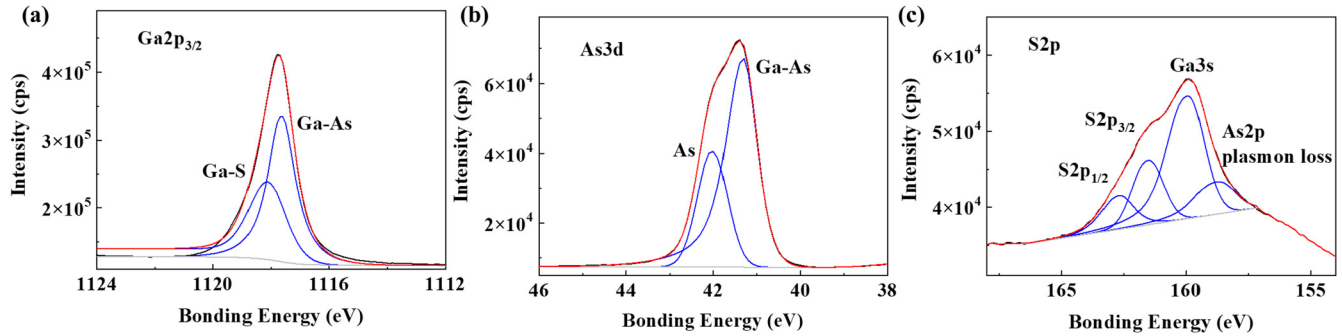


FIG. 2. (a) Ga 2p, (b) As 3d, and (c) S 2p core-level XPS spectra of S-passivated GaAs surfaces.

annealing. By varying the annealing temperature, different doping concentrations were attained, enabling us to investigate the impact of sulfur doping on the electrical properties of GaAs. The sheet resistances (R_s) of the samples were obtained from van der Pauw measurements. Figure 3(a) shows the dependence of sheet resistance on various RTA parameters. The sheet resistance drops dramatically from $\sim 2.1 \times 10^4$ to $79 \Omega/\text{sq}$ as the annealing temperature and time increase. The decrease in sheet resistance means more dopants have diffused into the GaAs lattice and are electrically activated. After removing the SiO_2 layer on the sample surface, the atomic force microscopy images were utilized to gain more information on surface morphologies and roughness of the blank sample and the sample annealed at 700°C for 5 min, as shown in Figs. 3(b) and 3(c). The root mean square (RMS) of the annealed surface roughness is only 0.32 nm, a little larger than the blank sample ($R_{\text{RMS}} = 0.24$ nm), which could be attributed to the S-S-dimer-terminated structure near the surface before the subsurface diffusion based on the thermal evolution of S-passivated GaAs studied in the previous literature.²¹ The roughness of these two samples changes little, which indicates a non-molten GaAs surface after thermal annealing treatment and do not affect the further electronic application.

We employed secondary ion mass spectrometry to probe the dopant profile after the RTA treatment (samples S1 and S2). Samples S1 and S2 were annealed using 700°C for 5 min and 750°C for 2 min, respectively. Among all samples, these two samples have the lowest sheet resistance. Both samples have a comparable dopant profile with a peak concentration of $\sim 4 \times 10^{20} \text{ cm}^{-3}$ at the surface, as shown in Fig. 3(d). The sulfur concentration declines rapidly from $\sim 4 \times 10^{20}$ to 10^{17} cm^{-3} within 50 nm. The dopants carried by the SAMM will limit the total number of dopants that can be possibly introduced into GaAs. Therefore, the dopants will follow the limited-source diffusion process at high temperature, which is described by Eq. (1),

$$N(x, t) = \left(\frac{N_0}{\sqrt{\pi Dt}} \right) \exp \left[- \left(\frac{x}{2\sqrt{Dt}} \right)^2 \right], \quad (1)$$

where N_0 represents the initial surface concentration, x denotes the diffusion distance, t is the annealing time, and D is the

diffusion coefficient, which varies with temperature. By fitting Eq. (1) into the data in Fig. 3(d), we find that the diffusion coefficient (D) for sulfur is $3.73 \times 10^{-16} \text{ cm}^2 \text{ s}^{-1}$ in sample S1 and $2.66 \times 10^{-15} \text{ cm}^2 \text{ s}^{-1}$ in sample S2, which is comparable to the widely observed value for sulfur in GaAs.²⁶ The variation in diffusion coefficient for these two samples is attributed to the difference in annealing temperature. Besides, the initial surface concentration (N_0) is determined to be $4.79 \times 10^{14} \text{ cm}^{-2}$, which is the total amount of sulfur dopant atoms transferred from the monolayer to the GaAs substrate. This value is slightly smaller than the results that Xia *et al.* reported (6.9×10^{14} S atoms cm^{-2}).²⁷ One possible reason for this discrepancy is that some sulfur atoms on the GaAs surface may diffuse into the SiO_2 capping layer during annealing in our case.

To obtain the electrical activation of the dopant atoms, we characterized the charge carrier transport at low temperature when a tunable magnetic field was applied perpendicular to the sample surface. Figure 4(a) shows the Hall resistance at 300 K under magnetic field. The Hall resistance is linearly correlated with the magnetic field from which we calculate the areal concentration of electrons as $3.72 \times 10^{14} \text{ cm}^{-2}$ following Eq. (2):

$$n_c = - \frac{\Delta B}{e \times (\Delta V_H / I)}, \quad (2)$$

where e is the elementary charge, V_H is the Hall voltage, I is the source current, B represents the magnetic field, and n_c is the free electron concentration per unit area. Given the electron concentration, we can further calculate the electron mobility at room temperature from the measured sheet resistance as $4274 \text{ cm}^2/\text{Vs}$ which is comparable to the literature reports. For example, Chiu *et al.*²⁸ reported the Hall mobility of $5018 \text{ cm}^2/\text{Vs}$ in the S-doped high electron mobility transistors. The mobility found by Lee *et al.* is $4120 \text{ cm}^2/\text{Vs}$ in the metal oxide semiconductor field-effect transistors.²⁶ For samples annealed at 650°C for 2 min and 750°C for 2 min (as shown in Fig. S1 in the supplementary material), the free electron concentration per unit area is 2.16×10^{11} and $4.73 \times 10^{14} \text{ cm}^{-2}$, respectively. The increases in the free electron concentration are attributed to longer annealing time and higher annealing temperature, which is also observed in the literature.²¹

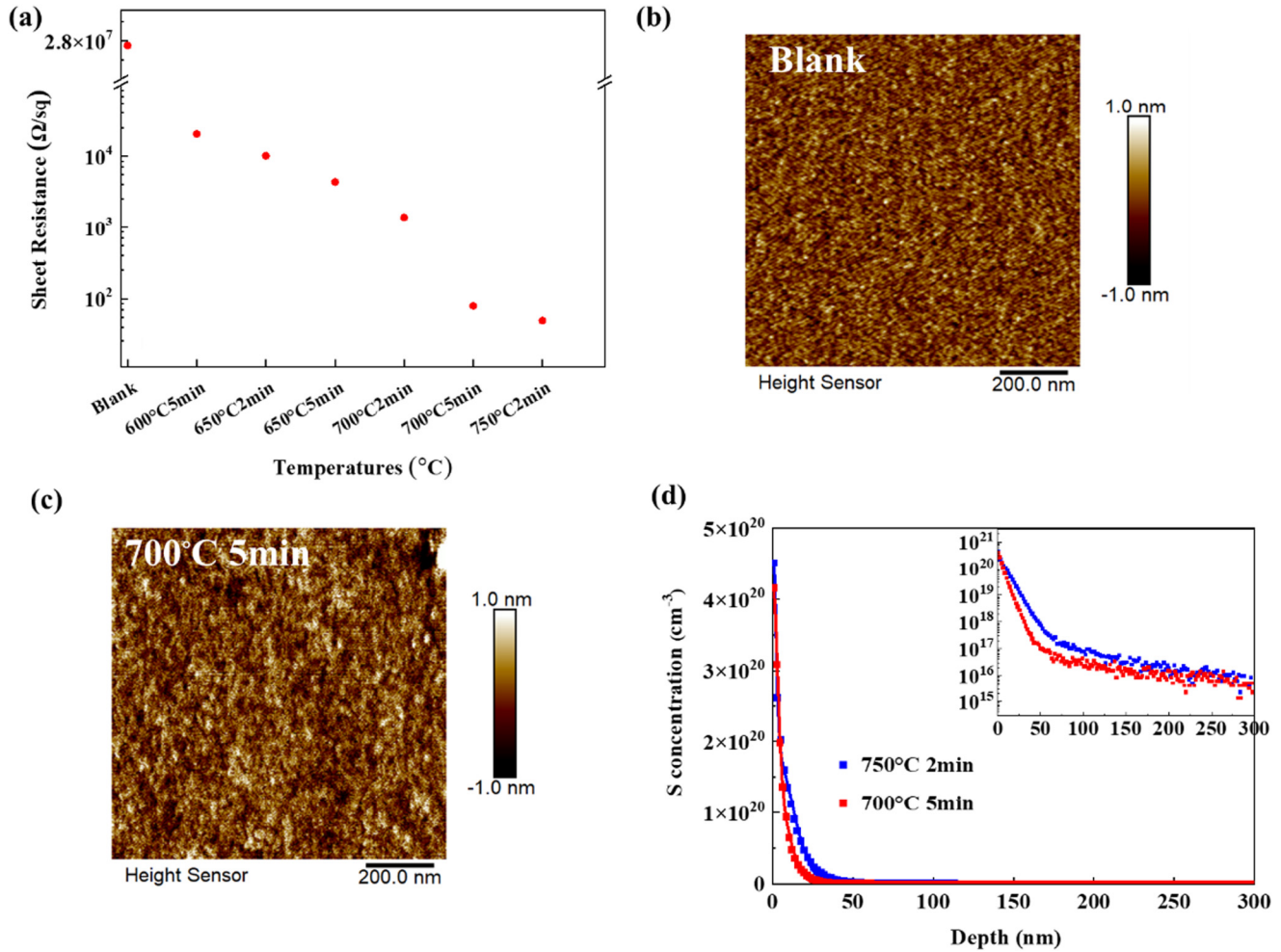


FIG. 3. (a) Sheet resistance of S-passivated GaAs with different annealing temperatures. The atomic force microscopy images of (b) the blank sample and (c) the sample annealed at 700 °C for 5 min. (d) SIMS doping profile of sulfur in samples S1 and S2. The solid line is a fitting line with Eq. (1).

To further investigate the characteristics of sulfur dopants, we conducted low-temperature Hall measurements (see Table S1 and Fig. S2 in the [supplementary material](#)) to investigate the electrical activity of sulfur dopants in GaAs. The temperature dependent electron concentration is plotted in Fig. 4(b). According to the dopant ionization theory we established previously,²⁹ the electron concentration is correlated with electrically active dopant concentration N_D and dopant ionization energy ΔE following Eq. (3):

$$n_c = \frac{-N_c + \sqrt{N_c^2 + 8N_c N_D \exp\left(\frac{\Delta E}{kT}\right)}}{4 \exp\left(\frac{\Delta E}{kT}\right)}, \quad (3)$$

where N_c is the effective density of states, defined as $N_c \approx 2 \left(\frac{2\pi m_n^* kT}{h^2} \right)^{3/2} = w(kT)^{3/2}$, with w being a constant related to the band structure of the semiconductor. By fitting Eq. (3) into the curve in Fig. 4(b) for the S-doped sample, we obtain that the activation energy of the sulfur dopants as 68 meV and the concentration of electrically active S donors as $4.4 \times 10^{14} \text{ cm}^{-2}$, which aligns well with the previous literature.³⁰ The low-temperature Hall measurements show that the sample has an activation energy of 68 meV, which is much larger than the reported S level (6 meV).³⁰ The activation energy we calculated from the temperature dependent electron concentration likely reflects both the shallow ionization energy level of S dopants and the deep energy level of interstitial N atoms. To demonstrate our hypothesis, we employed SIMS to analyze the nitrogen profile in GaAs, as shown in Fig. S3 in the [supplementary material](#). The nitrogen atoms can diffuse

24 March 2025 11:22:25

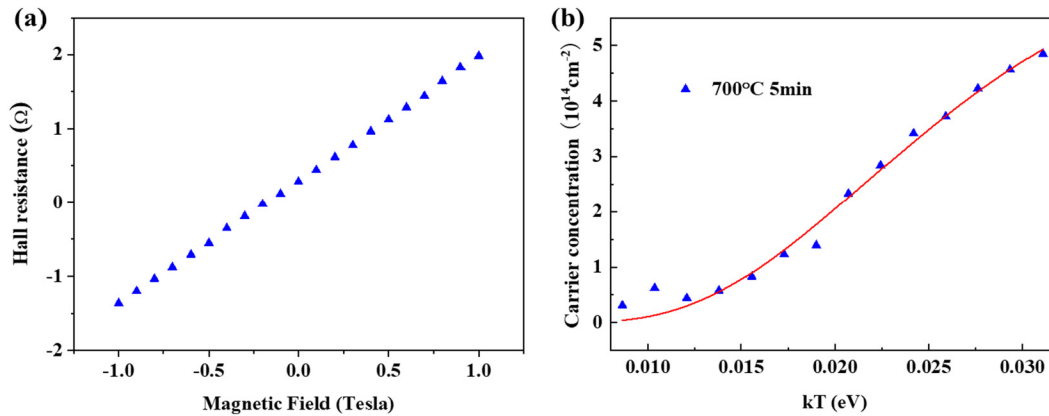


FIG. 4. (a) Hall resistance of S-treated GaAs annealed at 700 °C for 5 min, measured by Hall measurement at room temperature. (b) Temperature dependence of the average free electron concentration for S-treated GaAs. The red line is a fitting line with Eq. (3).

into GaAs during the annealing process. We previously found that the total number of sulfur dopants in GaAs is $4.79 \times 10^{14} \text{ cm}^{-2}$. Therefore, over 91% ($=4.4/4.79$) of dopants in GaAs introduced by the self-assembled molecular monolayer are electrically active. This indicates that the contamination brought in by the carrying molecules is minimal and the monolayer doping technique is a reasonably good technology that will likely find commercial applications.

As a further step, we fabricated a p-n junction diode on p-type GaAs (doped with Zn at a concentration of $\sim 10^{19} \text{ cm}^{-3}$) by the SAM sulfur monolayer doping process, details seen in S1 in the [supplementary material](#). We then measured the current-voltage characteristics of the p-type GaAs and S-doped p-GaAs, as shown in Fig. 5. The current is linear with voltage for p-type GaAs, indicating a good ohmic contact. However, the device of S-doped p-GaAs shows a typical rectifying behavior with a rectification ratio of up to 10^4 at $\pm 0.6 \text{ V}$ bias and an ideality factor of

1.26, indicating the high quality of the fabricated junction. Considering the Zn concentration in the p-type GaAs and the S concentration profile in Fig. 3(d), the junction depth of this fabricated p-n junction is defined as 21 nm. The reverse leakage current of our fabricated device is a little higher due to the uniform sulfur doping. However, this non-uniform doping is not unique for our monolayer doping but common for most doping techniques including ion implantation and thermal diffusion. The minority carrier lifetime (τ) is defined as $\tau = \frac{q n_i W_d}{2 J_d}$, where q is the unit charge, n_i is the intrinsic carrier concentration ($2.3 \times 10^6 \text{ cm}^{-3}$ in GaAs), W_d is the width of depletion region (15 nm), and J_d is the reverse saturation current density [$3.75 \times 10^{-7} \text{ A/cm}^2$ as shown in Fig. 5(b)]. The minority carrier lifetime in our fabricated p-n junction diode is calculated to be 1.48 ps, which is much smaller than that in reported GaAs.³¹ This is mainly attributed to the interstitial nitrogen atoms in GaAs, as investigated in the SIMS nitrogen results.

24 March 2025 11:22:25

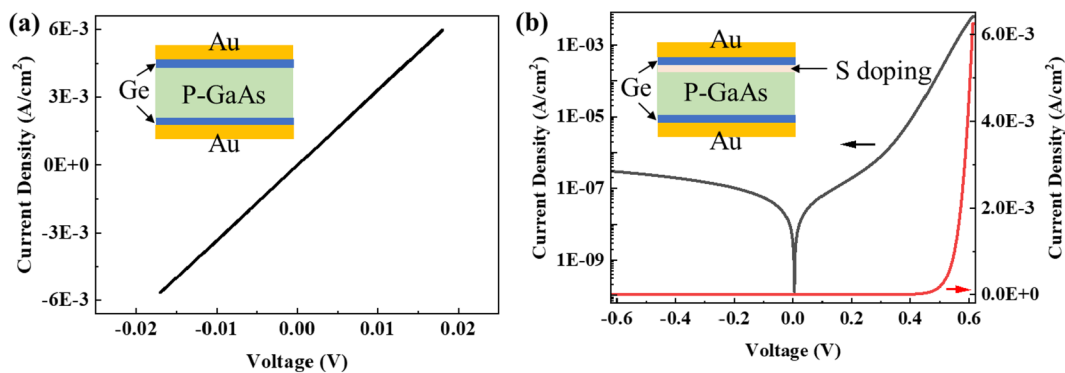


FIG. 5. (a) Current-voltage characteristics a p-type GaAs substrate. Inset: device diagram. (b) Current density vs voltage after the p-type substrate is doped with the self-assembled sulfur monolayer. Inset: diagram of the PN junction diode. The black curve is in the log scale and the red curve is in the linear scale.

CONCLUSION

In conclusion, we successfully grafted a sulfur monolayer onto the surface of GaAs. Sulfur dopants were successfully transferred into GaAs by rapid thermal annealing. We found over 91% of all opants in GaAs are electrically active. The contamination brought in by the self-assembly molecular monolayer doping has limited impact on the electrical activities of sulfur dopants in GaAs. To demonstrate the effective of this doping technique, we successfully fabricated a high-quality p–n junction diode on the p-type GaAs (doped with Zn) with the ideality factor of 1.26. This work demonstrates that the self-assembled molecule monolayer doping technique can be potentially find commercial applications in III–V transistors, high-speed nanoelectronics, and solar energy harvesting.

SUPPLEMENTARY MATERIAL

See the [supplementary material](#) that includes the normalized SIMS profiles in GaAs, a vital measurement to analyze the contamination in GaAs, the temperature dependent hall resistance and free carrier concentration of S-doped GaAs, a vital physical quantity that characterizes the electrically active concentration and donor energy level of S-doped GaAs, and the description of the fabrication of p–n junction.

ACKNOWLEDGMENTS

This work was financially supported by the National Science Foundation of China (NSFC) (Nos. W2412118, 62304131, U23A20350, and 92065103), the Oceanic Interdisciplinary Program of Shanghai Jiao Tong University (No. SL2022ZD107), the Shanghai Jiao Tong University Scientific and Technological Innovation Funds (No. 2020QY05), and the Shanghai Pujiang Program (No. 22PJ1408200). The devices were fabricated at the Center for Advanced Electronic Materials and Devices (AEMD), and Hall measurements were conducted at the Instrumental Analysis Center (IAC), Shanghai Jiao Tong University.

AUTHOR DECLARATIONS

Conflict of Interest

The authors have no conflicts to disclose.

Author Contributions

Zhengfang Fan: Formal analysis (lead); Investigation (lead). **Yumeng Liu:** Formal analysis (supporting). **Yizhuo Wang:** Formal analysis (supporting). **Hao Wei:** Resources (supporting). **He Li:** Resources (supporting). **Shuwen Guo:** Funding acquisition (equal); Investigation (equal). **Li He:** Resources (equal). **Xiaochun Lai:** Resources (supporting). **Yaping Dan:** Data curation (equal); Formal analysis (equal); Funding acquisition (equal); Investigation (lead).

DATA AVAILABILITY

The data that support the findings of this study are available within the article and its [supplementary material](#).

REFERENCES

- ¹S. Chang, J. He, S. Prucnal, J. Zhang, J. Zhang, S. Zhou, M. Helm, and Y. Dan, *ACS Appl. Mater. Interfaces* **14**, 30000 (2022).
- ²B. A. Sheriff, D. Wang, and J. R. Heath, *Nano Lett.* **6**, 1096 (2006).
- ³J. C. Ho, R. Yerushalmi, Z. A. Jacobson, Z. Fan, R. L. Alley, and A. Javey, *Nat. Mater.* **7**, 62 (2007).
- ⁴X. Gao, B. Guan, A. Mesli, K. Chen, and Y. Dan, *Nat. Commun.* **9**, 118 (2018).
- ⁵X. Wang, J. A. Hagmann, P. Nambodiri, J. Wyrick, K. Li, R. E. Murray, A. Myers, F. Misencosen, M. D. Stewart, C. A. Richter, and R. M. Silver, *Nanoscale* **10**, 4488 (2018).
- ⁶K. Li, J.-Y. Zhang, S. Chang, H. Wei, J.-J. Zhang, and Y. Dan, *ACS Appl. Electron. Mater.* **3**, 3346 (2021).
- ⁷L. Huang, Q. Mao, Z. Xiang, D. Zhu, and J. Meng, *IEEE Trans. Device Mater. Reliab.* **23**, 198 (2023).
- ⁸Y.-S. Ghee, B.-K. Kim, S.-I. Park, J. Song, W.-S. Kim, M.-H. Bae, and N. Kim, *Appl. Phys. Lett.* **122**, 4 (2023).
- ⁹N. Li, E. S. Harmon, J. Hyland, D. B. Salzman, T. P. Ma, Y. Xuan, and P. D. Ye, *Appl. Phys. Lett.* **92**, 14 (2008).
- ¹⁰I. A. Prudaev, S. N. Vainshtein, M. G. Verkholetoev, V. L. Oleinik, and V. V. Kopyev, *IEEE Trans. Electron Devices* **68**, 57 (2021).
- ¹¹R. Yan, D. Gargas, and P. Yang, *Nat. Photonics* **3**, 569 (2009).
- ¹²M. Hediéh, A. Salehi, and V. R. Mastelaro, *Russ. J. Electrochem.* **57**, 471 (2021).
- ¹³J. O'Connell, E. Napolitani, G. Impellizzeri, C. Glynn, G. P. McGlacken, C. O'Dwyer, R. Duffy, and J. D. Holmes, *ACS Omega* **2**, 1750 (2017).
- ¹⁴N. Tajik, A. C. E. Chia, and R. R. LaPierre, *Appl. Phys. Lett.* **100**, 20 (2012).
- ¹⁵S. Subramanian, E. Y. J. Kong, D. Li, S. Wicaksono, S. F. Yoon, and Y.-C. Ye, *IEEE Trans. Electron Devices* **61**, 2767 (2014).
- ¹⁶M. J. Jackson, B. L. Jackson, and M. S. Goorsky, *J. Appl. Phys.* **110**, 10 (2011).
- ¹⁷D. Cuypers, C. Fleischmann, D. H. van Dorp, S. Brizzi, M. Tallarida, M. Müller, P. Hönicke, A. Billen, R. Chintala, T. Conard, D. Schmeißer, W. Vandervorst, S. Van Elshocht, S. Armini, S. D. Gendt, and C. Adelman, *Chem. Mater.* **28**, 5689 (2016).
- ¹⁸J. C. Ho, A. C. Ford, Y.-L. Chueh, P. W. Leu, O. Ergen, K. Takei, G. Smith, P. Majhi, J. Bennett, and A. Javey, *Appl. Phys. Lett.* **95**, 7 (2009).
- ¹⁹K. R. Kort, P. Y. Hung, P. D. Lysaght, W.-Y. Loh, G. Bersuker, and S. Banerjee, *Phys. Chem. Chem. Phys.* **16**, 14 (2014).
- ²⁰J. H. Yum, H. S. Shin, R. Hill, J. Oh, H. D. Lee, R. M. Mushinski, T. W. Hudnall, C. W. Bielawski, S. K. Banerjee, W. Y. Loh, W.-E. Wang, and P. Kirsch, *Appl. Phys. Lett.* **101**, 25 (2012).
- ²¹E. C. Mattson and Y. J. Chabal, *J. Phys. Chem. C* **122**, 8414 (2018).
- ²²C. Zhang, M. Peng, W. Hu, and Y. Dan, *ACS Appl. Electron. Mater.* **2**, 275 (2020).
- ²³C. Zhang, S. Chang, and Y. Dan, *Adv. Phys. X* **6**, 1 (2021).
- ²⁴Z. H. Lu, M. J. Graham, X. H. Feng, and B. X. Yang, *Appl. Phys. Lett.* **62**, 2932 (1993).
- ²⁵G. Y. Gu, E. A. Ogryzlo, P. C. Wong, M. Y. Zhou, and K. A. R. Mitchell, *J. Appl. Phys.* **72**, 762 (1992).
- ²⁶J.-L. Lee, *J. Appl. Phys.* **85**, 807 (1999).
- ²⁷W. N. L. H. Xia, G. R. Massoumi, J. J. J. van Eck, L. J. Huang, W. M. Lau, and D. Landheer, *Surf. Sci.* **324**, 159 (1995).
- ²⁸H.-C. Chiu, Y.-C. Huang, C.-W. Chen, and L.-B. Chang, *IEEE Trans. Electron Devices* **55**, 721 (2008).
- ²⁹B. Guan, H. Siampour, Z. Fan, S. Wang, X. Y. Kong, A. Mesli, J. Zhang, and Y. Dan, *Sci. Rep.* **5**, 1 (2015).
- ³⁰E. F. Schubert, *Doping in III-V Semiconductors* (E. Fred Schubert, 2015), p. 165.
- ³¹M. Niemeier, J. Ohlmann, A. W. Walker, P. Kleinschmidt, R. Lang, T. Hannappel, F. Dimroth, and D. Lackner, *J. Appl. Phys.* **122**, 11 (2017).